A modelling methodology for robust stability analysis of non-linear electrical power systems under parameter uncertainties

Sharmila Sumsurooah, Milijana Odavic, *Member, IEEE,* and Serhiy Bozhko, *Member, IEEE*

***Abstract*—This paper develops a modelling method for robust stability analysis of non-linear electrical power systems over a range of operating points and under parameter uncertainties. Standard methods can guarantee stability under nominal conditions but do not take into account any uncertainties of the model. In this work, stability is assessed by using structured singular value (SSV) analysis also known as μ analysis. This method provides a measure of stability robustness of linear systems against all considered sources of structured uncertainties. The aim of this work is to apply the SSV method for robust small-signal analysis of non-linear systems over a range of operating points and parameter variations. To that end, a modelling methodology is developed to represent any such system with an equivalent linear model that contains all system variability, in addition to being suitable for μ analysis. The method employs symbolic linearisation around an arbitrary operating point. Furthermore, in order to reduce conservativeness in the stability assessment of the non-linear system, the approach takes into account dependencies of operating points on parameter variations. The methodology is verified through μ analysis of the equivalent linear model of a 4 kW permanent magnet machine drive, which successfully predicts the destabilising torque over a range of different operating points and under parameter variations. Further, the predictions from μ analysis are validated against experimental results.**

***Index Terms*—Robust stability analysis, Linear fractional transformation, Structured singular value, μ analysis.**

I. Introduction

THE More-Electric Aircraft (MEA) is a fast-developing technological trend in the aircraft industry. The MEA will have a more complex electrical distribution system with a multiplicity of power electronics converters interfaced loads [1]. It is well known that these loads, when tightly controlled, present a negative impedance to the source and thus can cause severe stability issues within the power system [2] [3]. Furthermore, the aircraft electrical power system (EPS) is subject to perturbations such as changes in environmental conditions or load demand. These uncertainties may lead to variation in system parameters and operating points which may further compromise system stability. Therefore it is crucial to incorporate parameter uncertainties in the stability assessment of an EPS and ensure system stability under all operating conditions especially for safety critical applications. However, due to non-linearities that are inherent in such systems, small-signal stability assessment may be challenging in the face of uncertainties. This is due to the fact that small-signal stability analysis is performed on a linear model about a certain operating point and depending on the amount of variability considered in the system, there may be an arbitrarily large number of linearised models to be generated and assessed. Hence, in order to apply robust small-signal stability assessment to non-linear systems, this paper develops a modelling methodology to represent a non-linear system by a generalised linear model that contains all system variability [4].

To assess small-signal system stability of power electronics systems, the major classical approaches that are generally employed are the eigenvalue-based method and the impedance-based methods such as Middlebrook criterion. Middlebrook criterion and many of its extensions such as the Gain and Phase Margin criterion and the Energy Source Analysis consortium (ESAC) criterion are based on the Nyquist criterion applied to the ratio of the source and load subsystem impedances [2] [5] [6]. An important drawback of the classical techniques is that they do not take into account system uncertainties such as parameter variations. However, in order to incorporate uncertainties in stability analysis, classical methods such as the eigenvalue method are combined with the Monte Carlo simulation. This probabilistic stability assessment approach can be employed to determine probability density functions of critical eigenvalues but cannot guarantee to identify the most critical system scenarios with respect to stability [7] [8]. Additionally, [9] presents an admittance space stability analysis method that incorporates uncertainties in the application of the classical ESAC criterion approach. Yet, the aforementioned methods involve exhaustive iterations of parameter variations, linearisation at a number of equilibrium points and computation of eigenvalues or impedances, which can be quite extensive. Nonetheless, [9] has developed a software to make the process automatic.

This paper employs the structured singular value (SSV, μ) approach which is applied to linear fractional transformation (LFT) based uncertain system models [10] [11] [12]. In addition to being a deterministic approach, SSV can provide a direct measure of stability robustness of a system with respect to its uncertain elements. Furthermore, SSV analysis is founded on the concept of an uncertain system model which defines system parameters not only in respect of their nominal values but also in terms of their possible variation about the nominal values. Hence, by working directly on an uncertain model, μ analysis eliminates the burden from a user of performing exhaustive iterations.

However, the SSV method is generally applied for robust stability analysis of a linear uncertain model with respect to a particular operating point. In view of applying the SSV method

to non-linear systems over a range of operating points, a number of methods have been proposed in the literature [13] [14]. A combined numerical and symbolic linearisation technique is presented in [13]. Another approach identifies the elements of state space matrices that vary with changes in operating conditions and system parameters, and then approximates those varying elements by polynomial functions [14]. Yet, these methods, similarly to the classical approach, cannot take into account dependencies of operating points on parameter uncertainties and may lead to conservative results. Nonetheless, it should be noted that these techniques were proposed for larger power systems.

The work proposed in this paper is based solely on symbolic linearisation around an arbitrary equilibrium point. It develops a general modelling approach to represent a non-linear system by an equivalent linear state space model in symbolic form that contains all defined system variability [13]. The approach explicitly expresses dependencies of operating points on system parameters, which can also be modelled as uncertainties. When compared to the aforementioned modelling approaches for SSV analysis, the developed modelling approach is less conservative since it preserves all parameter dependencies. In addition, it eliminates the need for exhaustive linearisation that is required by classical techniques.

The proposed modelling approach is applied to assess stability of a 4 kW permanent magnet (PM) machine drive. The methodology is validated through μ analysis of the system, which is used to predict the destabilising torque over a range of different operating points and under parameter variations. The stability of the PM machine system was analysed based on the classical eigenvalue method and also tested experimentally by the authors in [15]. The experimental results have been used to validate the predictions from μ analysis, presented in this paper [15].

II. Theoretical Background

In this work, the SSV approach is employed to determine whether a system remains robustly stable in the face of parametric uncertainties. The system to be analysed must be expressed in the LFT form prior to SSV analysis. [10] [16].

A. Linear fractional transformation

LFT is a modelling technique which is employed to "pull out" the indeterminate part from the known part of a system model and place it in the feedback form. If a general uncertain parameter P is considered to be bounded in the region [P_{min},P_{max}], it may be represented in its normalised form δ_P bounded within $[-1, 1]$. It is easy to show that P can be modelled as an LFT in δ_P in the expression (1) and in the matrix form in Fig. 1 [11] [12] [16].

$$P = P_o + P_o P_{var} \delta_P, \quad \delta_P \in [-1, 1] \tag{1}$$
$$\textit{where} \quad P_o = (P_{min} + P_{max})/2$$
$$\textit{and} \quad P_{var} = (P_{max} - P_{min})/(P_{max} + P_{min})$$

Similarly, the model of an entire system with parametric uncertainties can be represented in the LFT form [16] [17]. For the purpose of illustration, a general uncertain system expressed in the state space form with input u and output y, as shown in Fig. 2, is considered. The elements of the state space matrix $\left(\begin{smallmatrix} A & B \\ C & D \end{smallmatrix}\right)$ are functions of either fixed or uncertain parameters. For instance, element A_{ij} of the state matrix A can be expressed as $A_{ij} = f_1(P_1, P_2 ... P_m)$ where P_1 to P_m denote uncertain parameters of the system [14]. Based on the technique of LFT, it is possible to extract the set of uncertainties in their normalised form and regroup them in the diagonal uncertainty matrix Δ as shown in Fig. 3 where Δ = $diag\{\delta_{P1}, \delta_{P2}, ..., \delta_{Pm}\}$. As a result, the initial state space matrix is expanded to accommodate two sets of inputs namely u_Δ and u_s and two sets of output y_Δ and y_s as shown in Fig. 3 [11] [18].

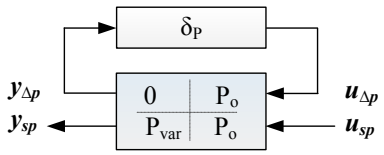

Fig. 1: Uncertain Parameter P as an LFT

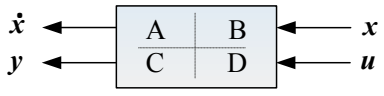

Fig. 2: The original uncertain system in state space form

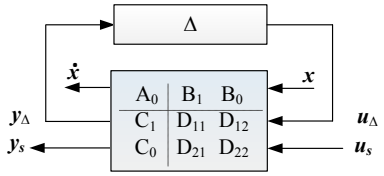

Fig. 3: The uncertain system with indeterminate uncertainties "pulled" out of the system

The expanded state space matrix can be simplified by absorbing the "states" through the use of equations (2) - (5). In this manner, the state space matrix in Fig. 3 is converted into the $N\Delta$ configuration in Fig. 4.

$$N_{11}(s) = C_1(sI - A_0)^{-1}B_1 + D_{11} \tag{2}$$
$$N_{12}(s) = C_1(sI - A_0)^{-1}B_0 + D_{12} \tag{3}$$
$$N_{21}(s) = C_0(sI - A_0)^{-1}B_1 + D_{21} \tag{4}$$
$$N_{22}(s) = C_0(sI - A_0)^{-1}B_0 + D_0 \tag{5}$$

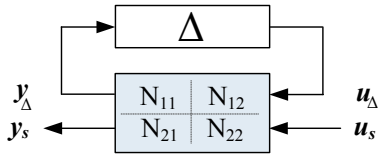

Fig. 4: Uncertain system in the $N\Delta$ or LFT form

Further, the system matrices in Fig. 4 can be represented as three distinct equations (6) - (8). By rearranging these equations to eliminate u_Δ and y_Δ and expressing the output y_s in terms of the input u_s, the transfer function of the system is obtained as (9). The uncertainty matrix Δ is clearly distinguishable in (9) and is said to have been "pulled out" of the original uncertain system. Equation (9) is known as the upper linear fractional transformation $F_u(N, \Delta)$. It is interesting to note that with the disturbance Δ being zero, the system is equivalent to $N_{22}(s)$, which is exactly the nominal transfer function of the uncertain system.

$$y_\Delta = N_{11}\ u_\Delta + N_{12}\ u_s \tag{6}$$

$$y_s = N_{21}\ u_\Delta + N_{22}\ u_s \tag{7}$$

$$u_\Delta = \Delta\ y_\Delta \tag{8}$$

$$F_u(N, \Delta) = \frac{y_s}{u_s} = N_{22} + N_{21}\Delta(I - N_{11}\Delta)^{-1}N_{12} \tag{9}$$

B. Structural singular value

Referring to the general LFT expression (9), it can be seen that the only source that can cause the system $N\Delta$ to become unstable is the feedback term $(I - M\Delta)^{-1}$ where $M = N_{11}$ [16]. With the assumption that the closed loop $M\Delta$ is initially stable, the structured singular value ($\mu_\Delta(M)$), as defined by (10), identifies the smallest uncertainty set, measured by $\bar{\sigma}(\Delta)$, that destabilises the system. At this point, the closed loop poles, which are given by $det(I - M\Delta)$, are at the imaginary axis [11] [19]. The SSV is a frequency-dependent matrix function which depends on both the system matrix $M(s)$ and the structure of Δ [11] [19].

$$\mu_\Delta(M) = \frac{1}{min[\bar{\sigma}(\Delta) : det(I - M\Delta) = 0, \Delta\ structured]} \tag{10}$$

The SSV theory gives necessary and sufficient conditions for stability robustness [10]. If $\mu_\Delta(M)$ is less than 1, it guarantees stability for the entire uncertainty set. However, it is computationally hard to obtain the exact value of $\mu_\Delta(M)$ [10] [20] [21]. Hence, lower and upper bounds on the structural singular value are computed instead. For simplicity, $\mu_\Delta(M)$ will be denoted as μ in the rest of this paper.

III. Modelling Methodology

This section describes the methodology for representing a non-linear system by an equivalent linear model which is valid for all operating points and parameter variations. The approach is illustrated by applying it to the PM machine drive system.

A. System structure

The power system under study is depicted by the circuit representation in Fig. 5. The system represents a hybrid distribution topology considered for the MEA power system [15]. The engine generator with the generator control unit, which is assumed to have an infinitely fast controller, is considered as an ideal 3-phase balanced voltage source. The transmission line from the power supply to the rectifier is modelled by an RL circuit. The six-pulse uncontrolled rectifier in Fig. 5, represents typically employed multiphase autotransformer-rectifier (ATRU) units of a real on-board system. It provides DC power to the surface mounted PM machine based electromechanical actuator (EMA) through an LC filter. The EMA is a standard vector-controlled PM motor drive depicted in Fig. 6 [15]. The parameters of the example power system are defined in Table I. With the assumption that the amplitude of the AC supply and the DC load current are constant and that commutation occurs only once during a commutation period, the power stage in Fig. 5 is modelled by the circuit in Fig. 7 by using the average-value modelling method [5] [22]. The six-pulse diode rectifier is modelled by the DC voltage source V_e in series with the equivalent resistance R_e and the equivalent inductance L_e which are given by (11) - (13). The transmission line inductance causes an overlap angle and hence a commutation voltage drop which is represented on the DC side by r_μ in (14) [15].

$$v_e = \frac{3\sqrt{3}\sqrt{2}}{\pi} v_s \tag{11}$$

$$R_e = r_\mu + r_F + 1.824 R_{eq} \tag{12}$$

$$L_e = L_F + 1.824 L_{eq} \tag{13}$$

$$r_\mu = \frac{3wL_{eq}}{\pi} \tag{14}$$

TABLE I: Nominal values for system parameters

Symbols	Units	Nominal Values	Description
v_s	V_{rms-ph}	223	phase source voltage
w	rad/s	$2\pi 50$	source frequency
R_{eq}	Ω	0.045	line resistance
L_{eq}	μH	60	line inductance
r_F	Ω	0.2	DC-link inductor resistance
L_F	mH	24.15	DC-link inductance
r_c	Ω	0.4	ESR of DC-link capacitor
C_F	μF	320	DC-link capacitance
w_{rated}	rpm	1140	rated speed
w_r^*	rpm	800	speed reference
T_{rated}	Nm	40	rated load torque
R_s	Ω	0.5	stator resistance
L_q	mH	2.3	stator leakage inductance
P	poles	20	number of poles
J_m	kgm^2	0.004	moment of inertia
F_m	Wb	0.123	constant flux of PM machine
K_{Pim}	-	4.124	current loop PI constant
K_{Iim}	-	3632	current loop PI constant
$w_{n,current}$	Hz	200	natural frequency of current loop
K_{Pw}	-	0.02	speed loop PI constant
K_{Iw}	-	0.863	speed loop PI constant
$w_{n,speed}$	Hz	10	natural frequency of speed loop
η	%	88.83	Efficiency of PM motor

B. Symbolic linearisation

The non-linear equations for the PM machine drive are given by (15) - (21) where $K_T = 3PF_m/4$ and $i_{cpl} = 3v_{sqm}^* i_{sqm}/4v_f$ [15]. The voltage across the DC-link capacitor

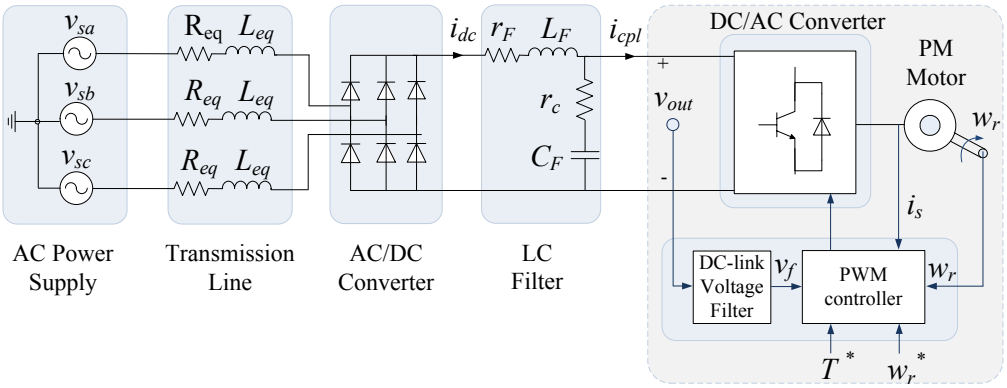

Fig. 5: Power system structure diagram

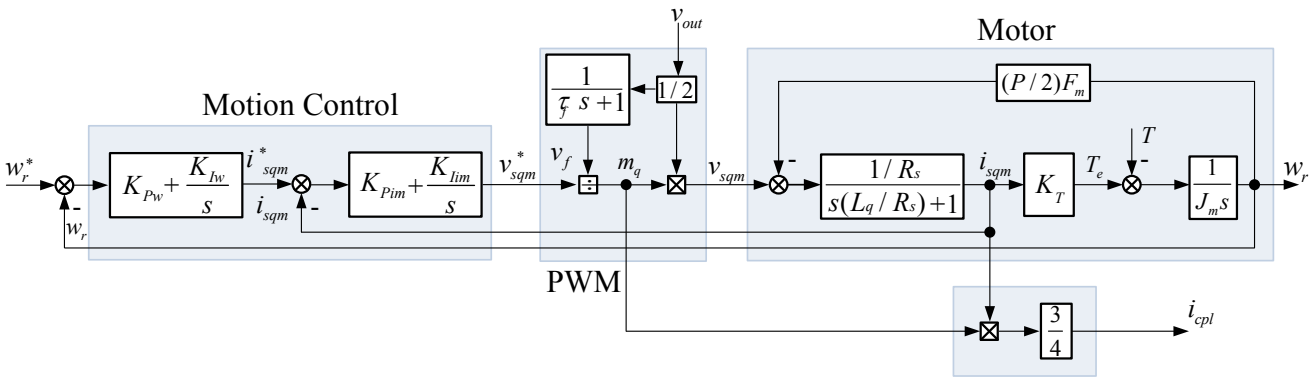

Fig. 6: Block diagram of the PM motor drive system

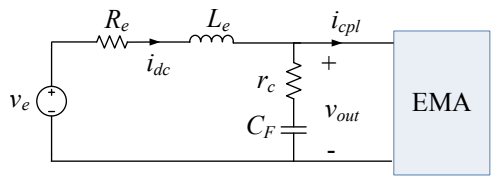

Fig. 7: Averaged model of the system in Fig. 5

is assumed to be equal to v_{out} given that the voltage drop across the ESR of the capacitor is very small.

$$\frac{di_{dc}}{dt} = -\frac{(r_c+R_e)}{L_e}i_{dc} + \frac{r_c}{L_e}i_{cpl} - \frac{v_{out}}{L_e} + \frac{v_e}{L_e} \quad (15)$$

$$\frac{dv_{out}}{dt} = \frac{1}{C_F}i_{dc} - \frac{1}{C_F}i_{cpl} \quad (16)$$

$$\frac{dw_r}{dt} = \frac{K_T}{J_m}i_{sqm} - \frac{1}{J_m}T \quad (17)$$

$$\frac{di_{sqm}}{dt} = -\frac{PF_m}{2L_q}w_r - \frac{R_s}{L_q}i_{sqm} + \frac{1}{2L_q}\frac{v^*_{sqm}v_{out}}{v_f} \quad (18)$$

$$\frac{dv_f}{dt} = -\frac{1}{\tau_f}v_f + \frac{1}{2\tau_f}v_{out} \quad (19)$$

$$\frac{dv^*_{sqm}}{dt} = -K_{Iim}i_{sqm} + K_{Iim}i^*_{sqm} - K_{Pim}\frac{di_{sqm}}{dt} + K_{Pim}\frac{di^*_{sqm}}{dt} \quad (20)$$

$$\frac{di^*_{sqm}}{dt} = -K_{Iw}w_r + K_{Iw}w^*_r - K_{Pw}\frac{dw_r}{dt} + K_{Pw}\frac{dw^*_r}{dt} \quad (21)$$

Prior to the linearisation of the system model, the non-linear equations are converted into a non-linear state space form where the vectors x, u and y denote system states, inputs and outputs respectively, and are given as:

$$x: \quad i_{dc},\, v_{out},\, w_r,\, i_{sqm},\, v_f,\, v^*_{sqm},\, i^*_{sqm}$$
$$u: \quad v_e,\, w^*_r,\, T$$
$$y: \quad v_{out}$$

An arbitrary equilibrium point is defined by X_o and U_o which denote steady state values of state vector x and input vector u respectively, and are given as:

$$X_o: \quad I_{dco},\, V_{outo},\, w_{ro},\, I_{sqmo},\, V_{fo},\, V^*_{sqmo},\, I^*_{sqmo}$$
$$U_o: \quad V_e,\, w^*_r,\, T_o$$

The input V_e and w^*_r are constant over all operating points. The load torque T is denoted as T_o at steady state. Finally, the non-linear state space system is linearised around equilibrium point (X_o,U_o) by using standard linearisation technique.

C. Expressing the state space matrix elements explicitly in terms of system parameters and inputs

This step involves expressing explicitly all elements of the resulting linearised state space model as functions of only

system parameters and inputs. Any indeterminate elements in the system model such as equilibrium points must be expressed in terms of definable system parameters and inputs.

For the system under study, firstly, X_o, as given by (22) - (28), is derived by setting (15) - (21) to zero.

$$\begin{aligned} I_{dco} &= I_{cplo} = 3V^*_{sqmo}I_{sqmo}/2V_{outo} && (22)\\ V_{outo} &= -R_eI_{dco} - V_e && (23)\\ w_{ro} &= w^*_r && (24)\\ I_{sqmo} &= T_o/K_T && (25)\\ V_{fo} &= V_{outo}/2 && (26)\\ V^*_{sqmo} &= V_{sqmo} = R_sI_{sqmo} + PF_mw_{ro}/2 && (27)\\ I^*_{sqmo} &= I_{sqmo} = T_o/K_T && (28) \end{aligned}$$

The steady state variables I_{dco} in (22) and V^*_{sqmo} in (27) are then further rearranged and expressed as (29) and (30). In addition, V_{outo} in (23) is expressed as (31) by using the constant power load equation $I_{dco} = P_o/V_{outo}$ where $P_o = T_ow_{ro}/\eta$.

$$I_{dco} = \frac{(3T_o/2K_T)(R_sT_o/K_T + PF_mw_{ro}/2)}{V_{outo}} \quad (29)$$

$$V^*_{sqmo} = R_sT_o/K_T + PF_mw_{ro}/2 \quad (30)$$

$$V_{outo} = \frac{V_e}{2}[1 + \sqrt{1 - \frac{4R_eT_ow_{ro}}{\eta V_e^2}}] \quad (31)$$

The flexibility of the linearised model, which now contains only determinate parameters and inputs in symbolic form, serves to cater for the system non-linearities.

D. Rational approximation of non-rational terms

Next, all non-rational elements in the linearised system model are expressed in their rational forms as is required for the conversion of the system model in its corresponding LFT configuration. In our case, the non-rational expression of V_{outo} in (31) is estimated in its rational form as in (32) by using the first two terms of the binomial expansion of the square root term in (31). The expression (32) is a good approximation of V_{outo} with respect to variations in torque as shown in Fig. 8.

$$V_{outo-est} = V_e - \frac{R_eT_ow_{ro}}{\eta V_e} \quad (32)$$

E. The equivalent linear model

After applying the above steps, the state space model $\left(\begin{smallmatrix} A & B \\ C & D \end{smallmatrix}\right)$, given by matrices (33) - (36), is obtained where V^*_{sqmo}, $V_{outo-est}$, A_{subs1} and A_{subs2} are given by (30), (32), (37) and (38) respectively. The developed model represents with good accuracy the system for all operating points and parameter variations, and is directly suited for μ analysis.

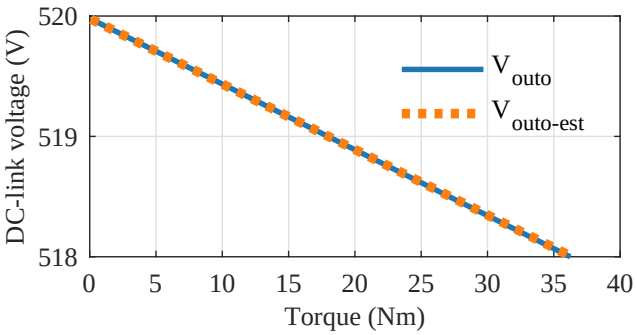

Fig. 8: Polynomial approximation of the steady state DC-link voltage V_{outo}

$$B = \begin{bmatrix} \frac{1}{L_e} & 0 & 0 \\ 0 & 0 & 0 \\ 0 & 0 & -\frac{1}{J_m} \\ 0 & 0 & 0 \\ 0 & 0 & 0 \\ 0 & K_{Pim}K_{Iw} & \frac{K_{Pim}K_{Pw}}{J_m} \\ 0 & K_{Iw} & \frac{K_{Pw}}{J_m} \end{bmatrix} \quad (34)$$

$$C = \begin{bmatrix} \frac{1}{L_e} & 0 & 0 & 0 & 0 & 0 & 0 \\ 0 & 1 & 0 & 0 & 0 & 0 & 0 \end{bmatrix} \quad (35)$$

$$D = \begin{bmatrix} 0 & 0 & 0 \end{bmatrix} \quad (36)$$

$$A_{susb1} = (-K_{Pim}K_{Iw} + \frac{K_{Pim}PF_m}{2L_q}) \quad (37)$$

$$A_{subs2} = -K_{Iim} - \frac{K_{Pim}K_{Pw}K_T}{J_m} + \frac{K_{Pim}R_s}{L_q} \quad (38)$$

F. The equivalent linear model suitable for μ analysis over a range of operating points and parameter variations

The equivalent linear model represents the non-linear system over a range of operating points and parameter variations. In order to illustrate this point, in this section, the nominal values of R_e and the speed reference w^*_r, denoted by R_{eo} and w^*_{ro}, have deliberately been set to 3.6 Ω and 3000 rpm respectively. The nominal torque T_{oo} is kept at 20 Nm and the other system parameters are defined as in Table I. These parameter values introduce more non-linearity in the system by causing a larger voltage drop in the DC-link voltage v_{out}. This increase in non-linearity better serves the purpose of illustration. It is worth noting that in practical systems, it is not improbable that the value of R_e is very high for cases where the lengths of interconnecting cables and input impedance of the power supply are more significant. Based on the new parameter values, the voltage V_{outo} is now better estimated by

$$A = \begin{bmatrix} -\frac{r_c+R_e}{L_e} & -\frac{1}{L_e} & 0 & \frac{3r_cV^*_{sqmo}}{2L_e\mathbf{V_{outo-est}}} & -\frac{3r_cT_oV^*_{sqmo}}{L_eK_T\mathbf{V^2_{outo-est}}} & \frac{3r_cT_o}{2K_TL_e\mathbf{V_{outo-est}}} & 0 \\ \frac{1}{C_F} & 0 & 0 & \frac{-3V^*_{sqmo}}{2C_F\mathbf{V_{outo-est}}} & \frac{3V^*_{sqmo}T_o}{C_FK_T\mathbf{V^2_{outo-est}}} & \frac{-3T_o}{2C_FK_T\mathbf{V_{outo-est}}} & 0 \\ 0 & 0 & 0 & \frac{K_T}{J_m} & 0 & 0 & 0 \\ 0 & \frac{V^*_{sqmo}}{L_q\mathbf{V_{outo-est}}} & \frac{-PF_m}{2L_q} & \frac{-R_s}{L_q} & \frac{-2V^*_{sqmo}}{L_q\mathbf{V_{outo-est}}} & \frac{1}{L_q} & 0 \\ 0 & \frac{1}{2T_f} & 0 & 0 & -\frac{1}{T_f} & 0 & 0 \\ 0 & \frac{-K_{Pim}V^*_{sqmo}}{L_q\mathbf{V_{outo-est}}} & A_{susb1} & A_{subs2} & \frac{2K_{Pim}V^*_{sqmo}}{L_q\mathbf{V_{outo-est}}} & \frac{-K_{Pim}}{L_q} & K_{Iim} \\ 0 & 0 & -K_{Iw} & \frac{-K_{Pw}K_T}{J_m} & 0 & 0 & 0 \end{bmatrix} \quad (33)$$

the third order binomial approximation, denoted by $V_{outoest3}$ and shown in Fig. 9.

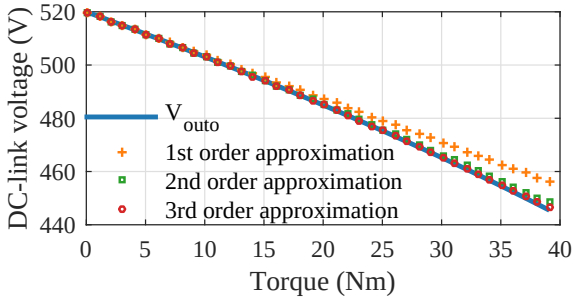

Fig. 9: Polynomial approximation of the steady state DC-link voltage V_{outo} with $R_e = 3.6\ \Omega$ and $w_r^* = 3000\ rpm$

Fig. 10 depicts a number of operating points of the system (I_{cplo},$V_{outo-est3}$) when both T_o and R_e are subject to variations. With R_e, w_r^* and T_o set to the aforementioned nominal values and the rest of the system parameters defined as in Table I, the nominal operating point can be shown to lie at the point Eq_{10} in Fig. 10. If R_e varies within $\pm$ 40% of R_{eo}, say due to changes in temperature, while $T_o = T_{oo} = 20\ Nm$, the operating point is seen to move to different positions along curve 1 in Fig. 10. On the other hand, if T_o varies within $\pm$ 90% of its nominal value while $R_e = R_{eo} = 3.6\ \Omega$, the operating point moves between Eq_{20} and Eq_{30}; Eq_{20} and Eq_{30} being the operating points corresponding to the minimum and maximum torque respectively. Hence, when both T_o and R_e vary, the operating points will lie between curves 2 and 3.

Thus, the generalised linear model converts to specific linear models about distinct operating points depending on the values assigned to the system parameters and inputs. Furthermore, the developed system model being linear is now suitable for μ analysis. Since the μ approach explicitly takes into account all varying system parameters and inputs, it becomes clear that in fact it assesses stability robustness of a non-linear system over all corresponding operating points, as will be demonstrated in the subsequent section.

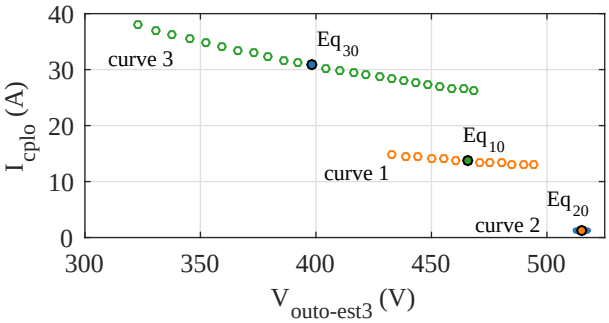

Fig. 10: Operating points with varying torque T_o and line resistance R_e

IV. Robust Stability Analysis under Load Uncertainty

In this section, μ analysis is applied to determine stability robustness of the power system shown in Fig. 5 when it is subject to uncertainty in load torque. The torque T_o is considered to vary within $\pm$90% of its nominal value of 20 Nm as depicted in Table II, while all other system parameters are assumed to be constant and equal to their nominal values as defined in Table I. The system is studied with no DC-link voltage filter. The destabilising load torque predicted by μ analysis is verified against experimental results.

TABLE II: Torque Uncertainty

Parameter	Average value (T_{oo})	Range of variation wrt average value (T_{var})
Torque (T_o)	20 Nm	$\pm$ 90%

A. Application of LFT

The application of μ analysis requires that the equivalent linear model be first converted in the $N\Delta$ or LFT form. Although the LFT operation can be done manually, the process can be laborious [12]. Fortunately, the LFT exercise as well as μ analysis can be performed automatically by employing

specialised software tools. MATLAB® Robust Stability Toolbox has been used in this work. The function 'robuststab(sys, omega)' performs both LFT operation and μ analysis on the state space system model denoted as 'sys' over the defined grid of frequencies denoted as 'omega'. For this case study, 'sys' is given by (33) - (36).

The operation of LFT involves firstly expressing all uncertain parameters in the system model as LFTs. The torque T_o, which is bounded in the interval [2 Nm, 38 Nm], can be represented as a perturbation in its normalised form δ_T bounded within [-1, 1]. Thus, T_o can be expressed as an LFT in δ_T based on (39) and the values in Table II [12] [23].

$$T_o = T_{oo} + T_{oo}T_{var}\delta_T, \quad \delta_T = [-1, 1] \tag{39}$$

From Fig. 11, which is an illustration of (39), it can be seen that when the 'perturbation' in torque is absent, $\delta_T = 0$, the torque is equal to its average value of $T_o = T_{oo} = 20$ Nm. When the 'perturbation' is at its maximum, either $\delta_T = -1$ at the low end of the uncertainty range where $T_o = T_{min} = 2$ Nm or $\delta_T = 1$ at the high end of the uncertainty range where $T_o = T_{max} = 38$ Nm. The critical torque, as represented by the point ($\delta_{T_{cr}}$, T_{cr}) in Fig. 11, will be determined by μ analysis in the next section.

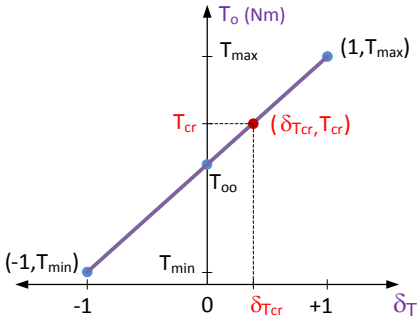

Fig. 11: Relationship between torque and the normalised disturbance in torque

Based on the LFT operation, all normalised parameters δ_T are then extracted from the system model (33) - (36) and grouped in a diagonal matrix in a feedback form. This results in the system model being converted in its $N\Delta$ form as shown in Fig. 4. The resulting disturbance matrix is given by (40) where δ_T appears 24 times since T_o appears that number of times in the uncertain system model.

$$\Delta(jw) = \delta_T I_{24\times 24} \tag{40}$$

It is worth noting that the order of an uncertainty matrix is dependent on the number of uncertain parameters as well as on the size and complexity of the power system being analysed. It also depends on the order of polynomial approximation of certain system elements such as V_{outo} in (32) for the system under study. Unfortunately, the higher the order of the uncertainty matrix, the higher is the computational burden [21]. Nevertheless, there exists some order reduction methods that can be used to minimise the size of these matrices [24].

B. Application of SSV

By applying SSV analysis to the system in its LFT form, the smallest disturbance matrix that causes instability is identified. MATLAB® Robust stability toolbox has been employed to compute μ bounds of the system under study [12] [17] [23]. The results of μ analysis, as depicted in Fig. 12, show the peak values of the lower and upper bounds of μ, which are in this case the same and equal to 2.38 at the frequency of 57 Hz. The critical frequency corresponds to the resonant frequency of the LC filter which can be estimated as $1/(2\pi\sqrt{L_F C_F})$. Based on the μ analysis results, the smallest destabilising disturbance matrix is extracted as in (41), and the robust stability margin is calculated as $min(\overline{\sigma}(\Delta)) = 1/\mu = 0.42$. The destabilising torque T_{cr}, computed from (42) and $\delta_{T_{cr}} = 0.42$, is equal to 27.6 Nm which is equivalent to the critical power of 2.6 kW.

$$\Delta_{cr}(j2\pi 57) = \delta_{T_{cr}}\, I_{24\times 24} = 0.42\, I_{24\times 24} \tag{41}$$

$$T_{cr} = T_{oo} + T_{oo}T_{var}\delta_{T_{cr}} \tag{42}$$

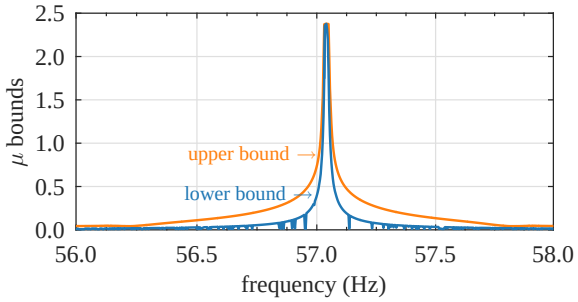

Fig. 12: μ chart for the determination of critical torque

The result, $\mu > 1$, indicates that the system is not robustly stable. The system does not remain stable over the whole uncertainty set (i.e. within 20 ± 18 Nm) but only from $T_{min} = 2$ Nm up to $T_{cr} = 27.6$ Nm. In this way, μ operates as a measure of stability robustness.

One known problem with μ analysis, as reported in the mathematical and engineering literature, is that the function μ can be discontinuous in cases where all the uncertain parameters are purely real [16] [17] [20]. This leads to a problem of convergence in the computation of a lower μ bound which fails to identify a critical disturbance matrix. It has been found that one way to solve the convergence problem is to add a small complex value (α) to the real parameters. This thus becomes a mixed μ problem instead of a purely real μ problem. This approach can significantly improve continuity and convergence of the lower bound. This solution can be justified from the engineering viewpoint given that some small dynamics are inherent and inevitable in practical systems [20] [25]. This problem was encountered at the outset of this study. Hence, a very small complexity of $\alpha = 0.1\%$ was added to the real parametric uncertainty by using the command "complexify" in MATLAB® Robust stability toolbox. This was sufficient to make the μ lower bound converge [12].

C. Simulation Results

The PM machine drive is modelled in the Simulink® environment to enable time-domain verification of the result from μ analysis. With the speed kept constant at 800 rpm, three values of torque are applied in steps to the model. At time $t = 4$ s, 95% of the critical torque (26.2 Nm) is applied to the system and the DC-link voltage $v_{out}(t)$ stabilises with time as can be seen in Fig. 13. At time $t = 8$ s, application of the critical torque $T_{cr} = 27.6$ Nm causes the system to reach boundary stability with sustained DC-link voltage oscillations. This confirms the results from μ analysis which predicted the critical torque of 27.6 Nm. Applying an additional torque of 5% over its critical value at $t = 12$s causes the system to become unstable as shown in Fig. 13.

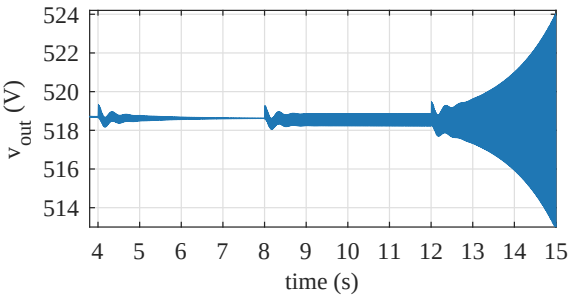

Fig. 13: Time domain simulation of DC-link voltage $v_{out}(t)$ at (i) t=4s, $T = 0.95T_{cr}$ (ii) t=8s, $T = T_{cr}$ (iii) t=12s, $T = 1.05T_{cr}$

D. Experimental Results

A number of experiments were undertaken on the PM machine drive test rig that is described in this work and were reported in [15]. It was found in the experiment that when the torque was increased to 26.7 Nm at a speed of 800 rpm, the DC-link voltage showed sustained oscillations as depicted in Fig. 10 in [15]. This is in very close agreement with the critical torque of 27.6 Nm determined from μ analysis. Thus, both experimental and simulation results confirm the validity of the proposed modelling approach.

E. Discussion

μ analysis directly provides an explicit measure of the amount of variability that is allowed in uncertain parameters for the system to remain stable. For the case under study, the robust stability margin equal to 0.42 implies that maintaining the normalised torque within 42 % of its nominal value ensures system stability. This information is very useful and can directly be employed in the design of the electrical power systems. For instance, in order to ensure that the system under study remains stable over the whole uncertainty range, μ should be less than 1. One way to do this is to limit the operating range to $T_o = 20$ Nm $\pm$ 38%. However, if the operating range is to be maintained within 20 Nm $\pm$ 90%, the input filter parameters L_F and C_F can be modelled as uncertainties in order to find their optimal values that will guarantee stability in the whole operating range.

Furthermore, the SSV method is less demanding for a user. The only inputs that are to be provided to the software are firstly nominal values and a variation range of uncertain parameters, and then an equivalent linear state space model.

In contrast, the classical eigenvalue approach applied in [15] to determine the critical torque of the PM machine drive is not direct and involves an extensive process. Firstly, the operating range is divided into a finite number of points. Then, for each operating point, numerical linearisation is performed and eigenvalues are calculated. The iterative process has to be further refined until the critical parameter value is obtained to a satisfactory accuracy.

The modelling methodology proposed in this work has been successfully applied to the power system under study. It is still to be tested on system-level architectures where source and load subsystems, of the order of the EPS under consideration, are interconnected. This aspect of the work is currently being investigated.

V. Effect of Parameter Variations on Stability Robustness

In the previous section, we found that stability can be guaranteed for the system under study up to the maximum power of 2.6 kW. In this section, the effect of parameter variations on the destabilising power is investigated by using the μ method that was described in section IV. In particular this analysis includes variations in system frequency, bandwidth of the DC-link voltage filter and natural frequency of the speed loop. All the other system parameters are kept constant as given in Table I unless specified otherwise. The results from μ analysis are verified against experimental results reported in [15].

A. System frequency

Some aircraft power system architectures are known to be "frequency-wild" with frequency changing in a wide range. It is important to analyse how stability robustness of the power system is affected by variations in system frequency. μ analysis is applied to determine the critical torque that destabilises the power system for system frequency ranging from 1 Hz to 300 Hz. For every frequency under study, the uncertain torque is as defined in Table II. The system is investigated with no DC-link voltage filter. The critical power is then computed from the critical torque, determined from μ analysis at each frequency point, based on $P = T_{cr} w_r/\eta$. Fig. 14 depicts the results from μ analysis. Further, a number of experiments were performed on the system to identify the destabilising power for frequencies of 50 Hz, 100 Hz, 200 Hz and 300 Hz. Fig. 14 shows the experimental results which have also been reported in Fig. 11 in [15]. There is a close agreement between the μ analysis predictions and the experimental results as can be seen in Fig. 14. It can be noted that an increase in system frequency causes an improvement in system stability.

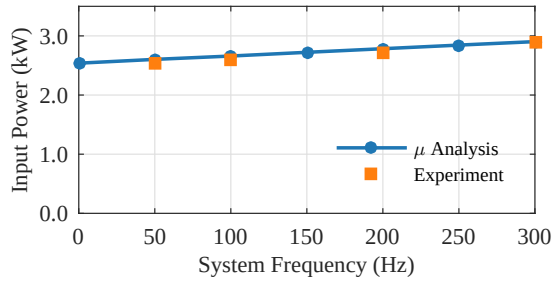

Fig. 14: Experimental and μ analysis-based critical power under conditions of varying system frequency

B. Bandwidth of the DC-link voltage filter

The DC-link voltage v_{out} is filtered for the computation of the modulation index in the digital signal processor (DSP) as shown in Fig. 6 [15]. The critical torque is determined for different values of the DC-link voltage filter (f_{cutoff}) ranging from 0 Hz to 300 Hz. The critical power is then computed from the critical torque, predicted by μ analysis at the different values of f_{cutoff}, based on $P = T_{cr} w_r$. Fig. 15 depicts the power stability threshold obtained from μ analysis. In addition, the critical power was measured experimentally at the shaft of the motor for f_{cutoff} of 10 Hz, 25 Hz, 50 Hz, 200 Hz and 300 Hz. Fig. 15 depicts the experimental results which have also been reported in Fig. 12 in [15]. These experimental results agree fairly well with μ analysis predictions as can be noted in Fig. 15. It can be noted that the effect of the DC-link voltage filter bandwidth on stability robustness is not monotonic and is around 75 Hz at the point where the system is the least robustly stable.

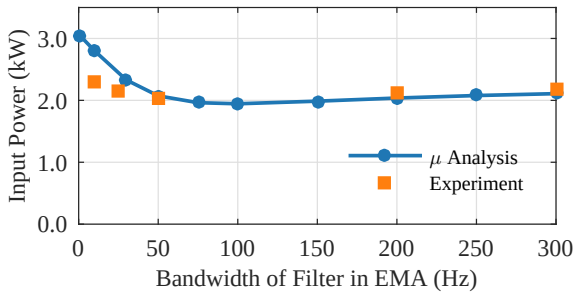

Fig. 15: Experimental and μ analysis-based critical power with varying bandwidth of the DC-link voltage filter

C. Natural frequency of the speed loop

μ analysis is applied to determine the destabilising power for different values of natural frequency of the speed loop (f_n) ranging from 1 Hz to 25 Hz. The DC-link voltage filter bandwidth is fixed at 50 Hz. Fig. 16 shows the results from μ analysis. Moreover, the critical power was measured experimentally at the shaft of the motor when f_n was set at 5 Hz, 10 Hz, 15 Hz and 20 Hz. Fig. 16 shows the experimental results which have also been reported in Fig. 13 in [15]. The experimental results agree closely with the μ analysis predictions as can be seen in Fig. 16. The system stability is seen to degrade with an increase in the natural frequency of the speed loop.

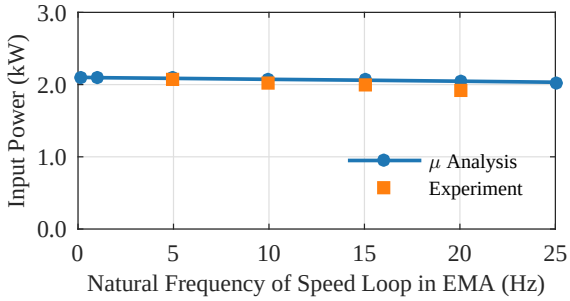

Fig. 16: Experimental and μ analysis-based critical power with varying natural frequency of the speed loop

D. Discussion

This section has demonstrated how parameter variations can affect system stability. The μ analysis results match closely the experimental results which were reported in [15] and also shown in Figs. 14 - 16 for the sake of completeness. This validates the methodology proposed in this paper.

VI. Conclusion

The aim of this work was to apply μ analysis to assess robust small-signal stability of a non-linear system over a range of operating points and under parameter uncertainties. To that end, a modelling methodology has been developed to represent a non-linear system by an equivalent linear system model that contains all defined system variability. This approach with respect to classical methods eliminates the need for exhaustive linearisation and extensive iterations under parameter variations. In addition, the modelling approach reduces conservativeness in stability assessment of a non-linear system as the equivalent linear model preserves all dependencies of operating points on parameter uncertainties of the system. The proposed modelling methodology has been verified through the SSV (μ) analysis of a 4 kW PM machine drive system, which successfully predicted the critical torque that causes system instability. The investigation included uncertainties in load and some system parameters. Further, all μ analysis predictions have been validated based on experimental results reported in [15]. Of note is that μ analysis, as compared to classical methods, can be employed to evaluate the effect of multiple parameter uncertainties acting simultaneously on system stability. This topic will be discussed in a future paper.

Acknowledgment

The authors gratefully acknowledge the support for the work from the EU as part of the Clean Sky project, part of EU FP7 program.

REFERENCES

[1] I. Moir and A. Seabridge, *Aircraft systems: mechanical, electrical and avionics subsystems integration*, vol. 52. John Wiley & Sons, 2011.

[2] R. D. Middlebrook, "Input filter considerations in design and application of switching regulators," *IAS Record, 1976*, 1976.

[3] A. B. Jusoh, "The instability effect of constant power loads," in *Power and Energy Conference, 2004. PECon 2004. Proceedings. National*, pp. 175–179, IEEE, 2004.

[4] S. Sumsurooah, M. Odavic, and S. Bozhko, "Development of lft-based models for robust stability analysis of a generic electrical power system over all operating conditions," in *Electrical Systems for Aircraft, Railway, Ship Propulsion and Road Vehicles (ESARS), 2015 International Conference on*, pp. 1–6, March 2015.

[5] K. Areerak, *Modelling and stability analysis of aircraft power systems*. PhD thesis, Department of Electrical and Electronic Engineering, University of Nottingham, UK, 2009.

[6] A. Riccobono and E. Santi, "Comprehensive review of stability criteria for DC power distribution systems," *Industry Applications, IEEE Transactions on*, vol. 50, no. 5, pp. 3525–3535, 2014.

[7] M. Kuhn, Y. Ji, and D. Schrder, "Stability studies of critical dc power system component for more electric aircraft using μ sensitivity," in *Control & Automation, 2007. MED'07. Mediterranean Conference on*, pp. 1–6, IEEE, 2007.

[8] J. Elizondo, R. Y. Zhang, J. K. White, and J. L. Kirtley, "Robust small signal stability for microgrids under uncertainty," in *Power Electronics for Distributed Generation Systems (PEDG), 2015 IEEE 6th International Symposium on*, pp. 1–8, IEEE, 2015.

[9] S. D. Sudhoff, S. F. Glover, P. T. Lamm, D. H. Schmucker, and D. Delisle, "Admittance space stability analysis of power electronic systems," *Aerospace and Electronic Systems, IEEE Transactions on*, vol. 36, no. 3, pp. 965–973, 2000.

[10] J. Doyle, "Analysis of feedback systems with structured uncertainties," in *IEE Proceedings D (Control Theory and Applications)*, vol. 129, pp. 242–250, IET, 1982.

[11] K. Zhou, J. Doyle, and K. Glover, *Robust and Optimal Control*. Feher/Prentice Hall Digital and, Prentice Hall, 1996.

[12] S. Sumsurooah, M. Odavic, and D. Boroyevich, "Modelling and robust stability analysis of uncertain systems," in *Proceedings of the 2013 Grand Challenges on Modeling and Simulation Conference*, p. 13, Society for Modeling & Simulation International, 2013.

[13] A. Varga, G. Looye, D. Moormann, and G. Gräbel, "Automated generation of lft-based parametric uncertainty descriptions from generic aircraft models," *Mathematical and Computer Modelling of Dynamical Systems*, vol. 4, no. 4, pp. 249–274, 1998.

[14] R. Castellanos, A. Messina, and H. Sarmiento, "Robust stability analysis of large power systems using the structured singular value theory," *International Journal of Electrical Power & Energy Systems*, vol. 27, no. 5, pp. 389–397, 2005.

[15] K.-N. Areerak, S. Bozhko, L. de Lillo, G. Asher, D. Thomas, A. Watson, and T. Wu, "The stability analysis of ac-dc systems including actuator dynamics for aircraft power systems," in *Power Electronics and Applications, 2009. EPE '09. 13th European Conference on*, pp. 1–10, Sept 2009.

[16] S. Skogestad and I. Postlethwaite, *Multivariable Feedback Control: Analysis and Design*. Multivariable Feedback Control: Analysis and Design, Wiley, 2005.

[17] G. J. Balas, J. C. Doyle, K. Glover, A. Packard, and R. Smith, "μ-analysis and synthesis toolbox: For use with matlab," 2001.

[18] R. B. Castellanos, C. T. Juarez, J. H. Hernandez, and A. R. Messina, "Robustness analysis of large power systems with parametric uncertainties," in *Power Engineering Society General Meeting, 2006. IEEE*, pp. 8 pp.–, 2006.

[19] M. Green and D. J. Limebeer, *Linear robust control*. Courier Dover Publications, 2012.

[20] A. Packard and J. Doyle, "The complex structured singular value," *Automatica*, vol. 29, no. 1, pp. 71–109, 1993.

[21] G. Ferreres, *A practical approach to robustness analysis with aeronautical applications*. Springer Science & Business Media, 1999.

[22] S. Sudhoff and O. Wasynczuk, "Analysis and average-value modeling of line-commutated converter-synchronous machine systems," *Energy Conversion, IEEE Transactions on*, vol. 8, no. 1, pp. 92–99, 1993.

[23] S. Sumsurooah, S. Bozhko, M. Odavic, and D. Boroyevich, "Stability and robustness analysis of a dc/dc power conversion system under operating conditions uncertainties," in *Industrial Electronics Society, IECON 2015 - 41st Annual Conference of the IEEE*, pp. 003110–003115, Nov 2015.

[24] A. Varga, "Balancing free square-root algorithm for computing singular perturbation approximations," in *Decision and Control, 1991., Proceedings of the 30th IEEE Conference on*, pp. 1062–1065, IEEE, 1991.

[25] D.-W. Gu, *Robust Control Design with MATLAB*, vol. 1. Springer, 2005.